
Recursive prestack depth migration using CFP-gathers¹

Jan Thorbecke²
A.J. Berkhout³

The Common Focus-Point Technology (CFP) describes prestack migration by two focusing steps: focusing in emission and focusing in detection. The output of the first focusing step represents a so-called CFP-gather. This gather defines a shot record that represents the subsurface response due to a focused source wavefield. We propose to apply the recursive shot record depth migration algorithm to the CFP-gathers of a seismic data volume, and will refer to this process as 'CFP-gather migration'. In the situation of complex geology and/or low signal to noise ratio, CFP-based image gathers are easier to interpret for non-alignment than the conventional image gathers. This makes the CFP-based image gathers better suited for velocity analysis. This important property will be illustrated by examples on the Marmousi model.

13.1 Introduction

Common Focus Point (CFP) gathers have been introduced by Berkhout (1992; 1997) and has been further developed in the DELPHI project of the University of Delft Thorbecke (1997). CFP technology has successfully been used for velocity independent redatuming Kelamis et

¹Published in Geophysics: Thorbecke, J. , and A. J. Berkhout, 2006, *Recursive prestack depth migration using CFP gathers*: Geophysics, **71** , no.6, S273-S283.

²E-mail: J.W.Thorbecke@tudelft.nl

³E-mail: A.J.Berkhout@tudelft.nl

al. (1999), estimation of Green's functions and velocity models Kabir and Verschuur (1997); Bolte et al. (1999); Hegge et al. (1999); Brisbourne et al. (2000) as well as to suppress internal multiples Berkhout and Verschuur (2000). In this Chapter the CFP technology is used for an alternative approach to shot record migration.

A CFP-gather can be considered as a shot record, the source of which is given by its focusing operator. Hence, a CFP-gather can be migrated by a generalized shot record migration algorithm, where the 'source wavefield' is given by the focusing operator and the 'shot record' by the CFP-gather. We will first set up a general framework for shot record migration and then integrate the CFP-gathers in this framework.

13.2 WRW model

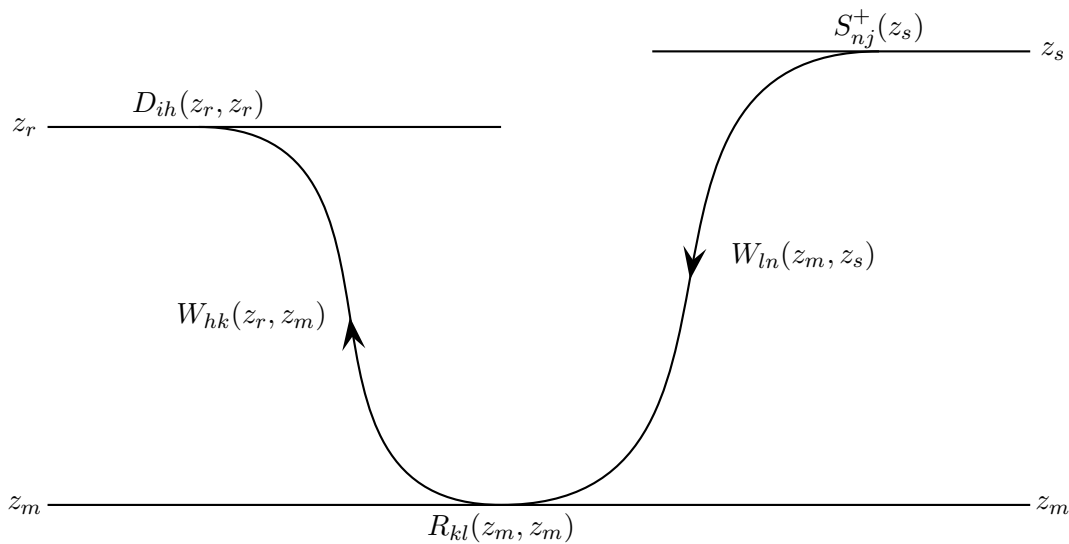


Fig. 13.1 One basic element of the **WRW** model, visualised by a raypath. In the continuous formulation, the propagation and reflection operators are integral kernels. In the discrete formulation they represent matrices. Note that depth levels z_s , z_r and z_m may be generalized to $z_s(x, y)$, $z_r(x, y)$ and $z_m(x, y)$.

The so-called **WRW** model is an attractive starting point for the derivation of new seismic processing algorithms. In this model wavefields are formulated in the (x, y, ω) -domain in terms of operators. In the discrete version, these operators represent vectors and matrices. Looking at primary wavefields only, we may write:

1. Down-going wavefield:

$$\mathbf{S}_j^+(z_m, z_s) = \mathbf{W}(z_m, z_s)\mathbf{S}_j^+(z_s) \quad (13.1a)$$

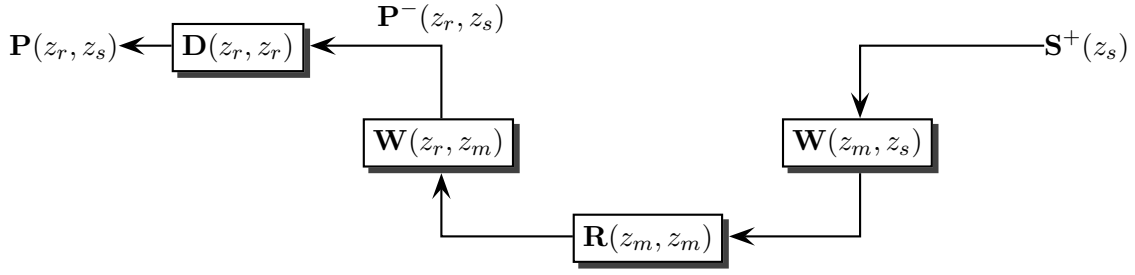


Fig. 13.2 WRW forward model for primary reflections, representing the 'inverse imaging equations' for seismic data. Note that in practice z_r and z_s often represent the acquisition surface z_0 , meaning that \mathbf{S}^+ and \mathbf{D} include the effect of the stress-free property of earth surface z_0 .

2. Up-going wavefields:

$$\Delta \mathbf{P}_j^-(z_r, z_s) = \sum_{m=1}^M \mathbf{W}(z_r, z_m) \mathbf{R}(z_m, z_m) \mathbf{S}_j^+(z_m, z_s) \quad (13.1b)$$

3. Measurements:

$$\Delta \mathbf{P}_j(z_r, z_s) = \mathbf{D}_j(z_r, z_r) \Delta \mathbf{P}_j^-(z_r, z_s). \quad (13.1c)$$

In the primary wavefield equations 13.1a,b and c detector matrix $\mathbf{D}_j(z_r, z_r)$ and source vector $\mathbf{S}_j^+(z_s)$ represent the angle-dependent acquisition information for one shot record (geometry, field arrays, source signature), j being the position of the source array. Matrices $\mathbf{W}(z_r, z_m)$ and $\mathbf{W}(z_m, z_s)$ quantify the angle-dependent *propagation* properties between all individual grid points of the acquisition surfaces z_r and z_s , and depth level z_m respectively (each row represents an upward and downward propagation operator respectively), and matrix $\mathbf{R}(z_m, z_m)$ quantifies the angle-dependent *reflection* properties for downward travelling waves (each column represents one reflection operator) at depth level z_m (see Figure 13.1). For a complex overburden, the columns of \mathbf{W} can define multi arrival events. The Δ , before \mathbf{P}_j in equation 13.1b, indicates reflection data without surface and internal multiples.

From the primary wavefield equations 13.1a,b,c it follows that the primary reflection measurements may also be written as (Figure 13.2):

$$\Delta \mathbf{P}_j(z_r, z_s) = \mathbf{D}_j(z_r, z_r) \Delta \mathbf{X}(z_r, z_s) \mathbf{S}_j^+(z_s), \quad (13.2a)$$

where matrix $\Delta \mathbf{X}(z_r, z_s)$ defines the earth's multidimensional transfer operators for primary reflections (each column represents one transfer operator):

$$\Delta \mathbf{X}(z_r, z_s) = \sum_{m=1}^M \mathbf{W}(z_r, z_m) \mathbf{R}(z_m, z_m) \mathbf{W}(z_m, z_s). \quad (13.2b)$$

Equations 13.2a and 13.2b are generally referred to as the **WRW** model Berkhout (1980). The **WRW** model presents a detail hiding formulation of wavefield measurements that include the influence of acquisition arrays as well as mode conversion.

13.3 Generalized shot record migration

The goal of migration is to remove the propagation effects of the primary wavefield and image the reflections at the correct positions in the subsurface. The generalized shot record migration algorithm (Berkhout, 1982, p. 218-220) is given by:

$$\mathbf{S}_j^+(z_m, z_s) = \mathbf{W}(z_m, z_s) \mathbf{S}_j^+(z_s) \quad (13.3a)$$

$$\mathbf{P}_j^-(z_m, z_s) = \mathbf{F}(z_m, z_r) \mathbf{P}_j^-(z_r, z_s), \quad (13.3b)$$

where equation 13.3a represents forward extrapolation of the source wavefield and equation 13.3b represents inverse extrapolation of the recorded wavefield. Note that \mathbf{P}_j contains all internal and free surface multiples. The extrapolated wavefields are related to the reflection information at depth level z_m by:

$$\mathbf{P}_j^-(z_m, z_s) = \mathbf{R}(z_m, z_m) \mathbf{S}_j^+(z_m, z_s). \quad (13.4)$$

From this equation the reflection information $\mathbf{R}(z_m, z_m)$ can be derived from $\mathbf{S}_j^+(z_m, z_s)$ and $\mathbf{P}_j^-(z_m, z_s)$ by matrix inversion.

Accurate extrapolation of wavefields is a computationally expensive task. By choosing the two wavefields \mathbf{S}_j^+ and \mathbf{P}_j^- in a clever manner, it is possible to do the shot record migration in a more efficient way. Let us first consider the recursive version of the shot record migration equations 13.3a,b.

13.3.1 Recursive extrapolation for shot record migration

The forward and inverse extrapolation matrices represented by \mathbf{W} and \mathbf{F} in the migration equations 13.3a and 13.3b, respectively, can be implemented in many different ways. To be able to handle the propagation through a complex subsurface a recursive extrapolation scheme in the space-frequency domain is used (Berkhout, 1982, p. 201-206):

$$\mathbf{W}(z_m, z_s) = \mathbf{W}(z_m, z_{m-1}) \mathbf{W}(z_{m-1}, z_{m-2}) \dots \mathbf{W}(z_1, z_s) \quad (13.5a)$$

$$\mathbf{F}(z_m, z_r) = \mathbf{F}(z_m, z_{m-1}) \mathbf{F}(z_{m-1}, z_{m-2}) \dots \mathbf{F}(z_1, z_r), \quad (13.5b)$$

where for every recursive inverse operator we use the approximation $\mathbf{F} = [\mathbf{W}^*]^T$. The rows of the recursive \mathbf{W} and \mathbf{F} matrices contain spatial convolution operators. These optimised finite-difference operators are calculated only once for the velocity and frequency range of interest and stored in a table. During the extrapolation, the operator needed for the current frequency and velocity at position (\mathbf{x}_i, z_m) is read from the table Blacquière (1989). For instance, one

extrapolation step from z_{m-1} to z_m is given by the space-variant convolutions:

$$\mathbf{S}_j^+(z_m, z_s) = \mathbf{W}(z_m, z_{m-1})\mathbf{S}_j^+(z_{m-1}, z_s) \quad (13.6a)$$

$$\mathbf{P}_j^-(z_m, z_s) = \mathbf{F}(z_m, z_{m-1})\mathbf{P}_j^-(z_{m-1}, z_s), \quad (13.6b)$$

where \mathbf{W} and \mathbf{F} are band matrices. For a detailed discussion about the calculation of short optimised extrapolation operators for 2- and 3-dimensional wavefield extrapolation the reader is referred to Holberg (1988) and Thorbecke et al. (2004).

13.3.2 Imaging principle for shot record migration

The reflection equation 13.4 shows that the reflectivity matrix, $\mathbf{R}(z_m, z_m)$, cannot be determined from one shot record, unless we assume that $\mathbf{R}(z_m, z_m)$ can be approximated by a diagonal matrix, $\hat{\mathbf{R}}(z_m, z_m)$ of 'effective' reflection coefficients. Effective reflection coefficients equals physical reflection coefficients if the reflection property at z_m is largely angle-independent or the incident wavefield is locally close to a plane wave, or both. Using the concept of effective reflection coefficients, we avoid full matrix inversion and the reflection equation 13.4 may be rewritten as:

$$\mathbf{P}_j^-(z_m, z_s) = \hat{\mathbf{R}}(z_m, z_m)\mathbf{S}_j^+(z_m, z_s), \quad (13.7a)$$

for each temporal frequency component. If we aim at *frequency-averaged* reflection coefficients, stable inversion of imaging equation 13.7a is given by

$$\hat{\mathbf{R}}_{ij}(z_m, z_m) = \frac{\sum_{\omega} \mathbf{P}_{ij}^-(z_m, z_s) [\mathbf{S}_{ij}^+(z_m, z_s)]^*}{\sum_{\omega} |\mathbf{S}_{ij}^+(z_m, z_s)|^2}, \quad (13.7b)$$

with i ranging along z_m and j ranging along z_s .

In addition, if we also aim at one *angle-averaged* reflection coefficient for each grid point (\mathbf{x}_i, z_m) , another summation can be carried out:

$$\hat{R}(\mathbf{x}_i, z_m) = \sum_j \frac{\sum_{\omega} \mathbf{P}_{ij}^-(z_m, z_s) [\mathbf{S}_{ij}^+(z_m, z_s)]^*}{\sum_{\omega} |\mathbf{S}_{ij}^+(z_m, z_s)|^2} \quad (13.7c)$$

the summation over j meaning a summation over all involved shot records.

For a given i , imaging equation 13.7b shows the images of the involved shot records (j is variable) of grid point (\mathbf{x}_i, z_m) . If the underlying velocity distribution is correct, these images are aligned and can be found at $t = 0$. If the process of extrapolation and imaging is applied for all depth levels of interest, the resulting images can be collected in an 'image gather' for lateral position \mathbf{x}_i (source position \mathbf{x}_j and depth position z_m are variable).

13.3.3 Recursive migration of CFP-gathers

Migration of CFP-gathers is similar to migration of shot records. Considering focusing in emission, a trace in a CFP-gather is computed by weighted summation (in phase and amplitude) along the sources in a common receiver gather in such a way that the constructed

wavefront $\mathbf{P}_j^-(z_r, z_f)$ originates from a notional source at point (x_j, z_f) in the subsurface. The CFP-gather for focusing in emission is given by:

$$\mathbf{P}_j^-(z_r, z_f) = \Delta \mathbf{P}(z_r, z_s) \mathbf{F}_j(z_s, z_f) \quad (13.8)$$

where $\mathbf{F}_j(z_s, z_f)$ is the focusing operator containing the weights in amplitude and phase. Considering the **WRW** model, the CFP-gather is a shot record with a focusing source array given by:

$$\mathbf{S}_j^+(z_s, z_f) = \mathbf{S}(z_s) \mathbf{F}_j(z_s, z_f). \quad (13.9)$$

The principle of combining shot gathers at the surface for the synthesis of areal source responses, also referred to as areal shot record technology, was introduced by Berkhout (Berkhout (1992)) and further investigated by Rietveld (1995). Extrapolation of the CFP-gather in equation 13.8 and the focusing source array in equation 13.9 from depth level z_{m-1} to depth level z_m can be represented by the recursive extrapolation equations 13.6a,b with z_s replaced by z_f :

$$\mathbf{S}_j^+(z_m, z_f) = \mathbf{W}(z_m, z_{m-1}) \mathbf{S}_j^+(z_{m-1}, z_f) \quad (13.10a)$$

$$\mathbf{P}_j^-(z_m, z_f) = \mathbf{F}(z_m, z_{m-1}) \mathbf{P}_j^-(z_{m-1}, z_f), \quad (13.10b)$$

To obtain the frequency-averaged reflection coefficients we can apply the same steps as we have done for the imaging principle for shot record migration, which leads to

$$\hat{\mathbf{R}}_{ij}(z_m, z_m) = \frac{\sum_{\omega} \mathbf{P}_{ij}^-(z_m, z_f) [\mathbf{S}_{ij}^+(z_m, z_f)]^*}{\sum_{\omega} |\mathbf{S}_{ij}^+(z_m, z_f)|^2}, \quad (13.11)$$

with i ranging along z_m and j now ranging along the level where focusing occurs, i.e. $z = z_f$. The receiver and source components in imaging equation 13.11 are given by extrapolation equations 13.10a and 13.10b. Imaging equation 13.11 contains source energy from *all* available shot records, which illuminate the focal point, while imaging equation 13.7b contains energy from *one* shot only. Therefore, imaging equation 13.11 is significantly more stable than imaging equation 13.7b, particularly around the focal point.

The summation over shot records j in imaging equation 13.7c adds more angle information of the same reflector and illuminates some extra parts due to the differences in source and receiver coordinates. Summation over migrated CFP-gathers in imaging equation 13.11 adds more complete imaging results at different focal points (\mathbf{x}_j, z_f) .

$$\hat{R}(\mathbf{x}_i, z_m) = \sum_j \frac{\sum_{\omega} \mathbf{P}_{ij}^-(z_m, z_f) [\mathbf{S}_{ij}^+(z_m, z_f)]^*}{\sum_{\omega} |\mathbf{S}_{ij}^+(z_m, z_f)|^2}. \quad (13.12)$$

If for the same image quality the number of focal positions can be chosen smaller than the number of shot records, a more efficient migration can be carried out.

The construction of a CFP gather from shot records is explained by using numerical data based on the model shown in Figure 13.3a. The numerical data is modeled with a fixed acquisition

spread where the source positions are defined at every receiver position (201 shot positions with $\Delta x = 15$ m). For the forward modeling of the data an acoustic finite difference algorithm is used.

The synthesis process for a focusing receiver with a focal point defined at the synclinal interface at $x = 0$ and $z = 950$ m (the focal point is indicated with a black bullet in Figure 13.3a) is shown in detail in Figure 13.3. The time reversed focusing operator for the defined focus is shown in Figure 13.3b. This operator is applied to all common shot gathers available. Three different common shot gathers with source positions at $x = -495$, $x = 0$ and $x = 495$ m are shown in Figure 13.3c, d and e respectively. Convolution along the time axis of the traces in the shot gathers, with the traces in the synthesis operator gives the intermediate synthesis results shown in Figure 13.3f, g and h. Note that in these intermediate synthesis results the bow-tie of the syncline interface is still present. Summation over all the traces in these results defines one trace of the CFP gather (figure 13.3i). The most important contribution in the integrated result is determined by the Fresnel zone related to the focal point. If the focusing operator is correct then the operator time at the source position is identical with the time of the event present in the CFP trace. The summed trace is placed in the CFP gather at the position of the source. By carrying out the convolution and integration along the traces in the gather for all shot gathers available the CFP gather for focusing in detection is constructed.

The events which are present in the shot record are also present in the intermediate synthesis result in Figure 13.3f, g and h. In Figure 13.3f four events are observed. The top event originates from the first reflector and can be regarded as a 'non-causal' event with respect to the focal point. The event with the triplication in it originates from the syncline boundary, the weak S-shaped event (indicated with ⊕) originates from a diffraction point (positioned at $x=-750$ $z=100$ m) and the last event originates from the deepest boundary. In the CFP gather shown in Figure 13.3i the reflection from the syncline (indicated by an arrow) and the deeper boundary are also visible. Due to the phase shift the response of the first reflector is present in the CFP-gather at negative times. The complex bow-tie response of the second reflector in the shot record (Figure 13.3d) has been reduced to a simple hyperbolic event in the CFP-gather.

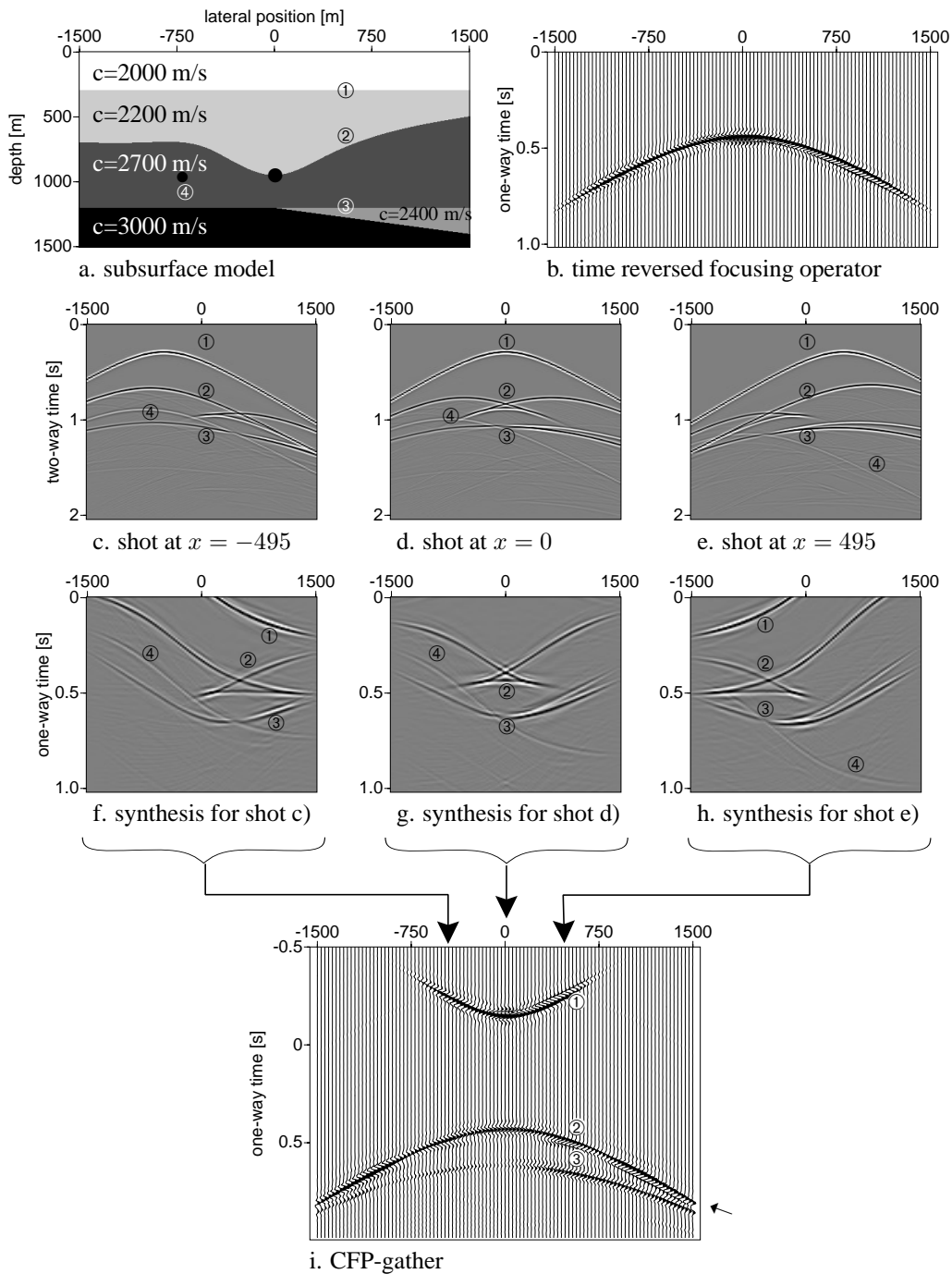


Fig. 13.3 Construction of a CFP-gather for focusing in detection. The focus point response has been indicated with an arrow in picture i, showing the same traveltime as the operator ('principle of equal traveltimes') in picture b. The focussing process transforms each shot record (pictures c, d and f) into one trace that is positioned in the CFP-gather at the source position of the corresponding shot record. The horizontal parts in picture f, g and h (Fresnel zones) contribute to the result in picture i. Note that the CFP-gather can be seen as a shot record with an areal source given by the focusing operator. Note also that the CFP-gather does not contain multi-arrival times: the spatial phase has been removed, leading to simpler events than in the original shot record (picture d).

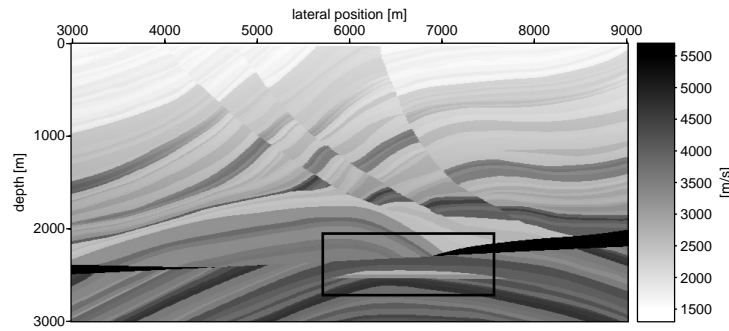


Fig. 13.4 The velocity model used to model the Marmousi data set. The frame indicates a potential hydrocarbon reservoir.

Based on a collection of CFP-gathers a CFP-offset section can be constructed by selecting from every CFP-gather a fixed offset from the focal point. To construct these gathers we make use of the Marmousi data set, which velocity model is shown in Figure (13.4).

The Marmousi data of the Institut Français du Pétrole is based on a complex geologic model Versteeg and Grau (1991). This data provides a challenge for any migration method, even when the correct velocities are used. The acquisition geometry is a marine type of acquisition (end of spread) containing 96 geophone groups, with a minimum offset of 200 m and a receiver spacing of 25 m. The modelled data contains 240 shots with a shot spacing of 25 m. A single trace has a length of 4 s with a sampling interval of 4 ms. The potential hydrocarbon reservoir is positioned around $x = 7000$ m, $z = 2500$ m and can be recognised by the horizontal levels in the turtle-back structure.

The pre-processing for the Marmousi data set was carried out in a twostep approach Rietveld (1995) in which the surface related multiples and the thin layer reverberations were removed. The missing near offsets were interpolated using a CMP interpolation technique. This pre-processed data set, including the interpolated offsets, was also used as input for the migration algorithms discussed below.

In Figures 13.5 and 13.6 CFP-offset gathers are compared with shot-based offset gathers. The main difference between the two sections is that in shot-based offset gathers the traces are single fold: only one trace out of a shot gather is used in the offset gather. In the CFP-based offset gathers every trace has been constructed using all the traces in a shot record. The CFP-offset gathers have therefore a higher quality and are easier to interpret. By choosing different focal levels, for example at $z = 3000$ m in Figure 13.6, deeper parts of the model can be better interpreted.

Figure 13.7 compares shot record migration with CFP-gather migration. Note the difference in illumination area (compare c with h and d with i) when the source is placed at the surface (shot-based) or the deep subsurface (CFP-based). It can also be seen that by using CFP gathers a target oriented approach around the chosen focal points is possible. Using CFP and imaging equations 13.8-13.11 it can be shown that the operator $\mathbf{F}_j(z_s, z_f)$ used to construct the CFP-

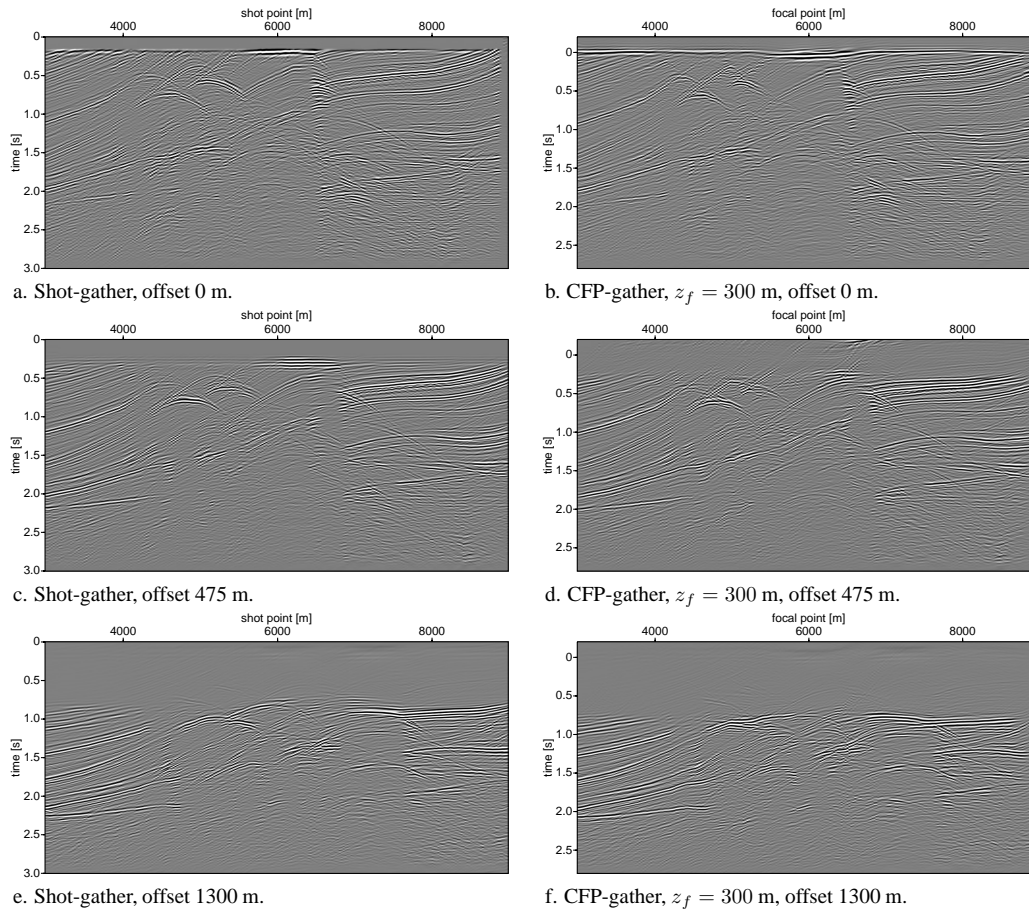


Fig. 13.5 Comparison between shot- and CFP-offset (focus depth $z_f = 300$ m) gathers. The CFP-offset gather can be considered as a redatumed data set, where the receiver positions have been inverse extrapolated to $z = 300$ m. The CFP-based offset gather has close to the sea-bottom a better quality than the shot-based offset gather.

gather cancels out in the final imaging result. This means that velocity errors in $\mathbf{F}_j(z_s, z_f)$ have no influence on the image gather. Thus one can choose any kind of focusing operator as long as the source and receiver gathers used in the migration are using the same focusing operator.

13.4 CFP-gather migration experiments

Several imaging experiments have been carried out to test and compare the image quality of CFP-gather migration with conventional migration of shot records in the presence of noise. For the migration and the construction of the focusing operators different velocity models have been used to illustrate the influence of velocity errors.

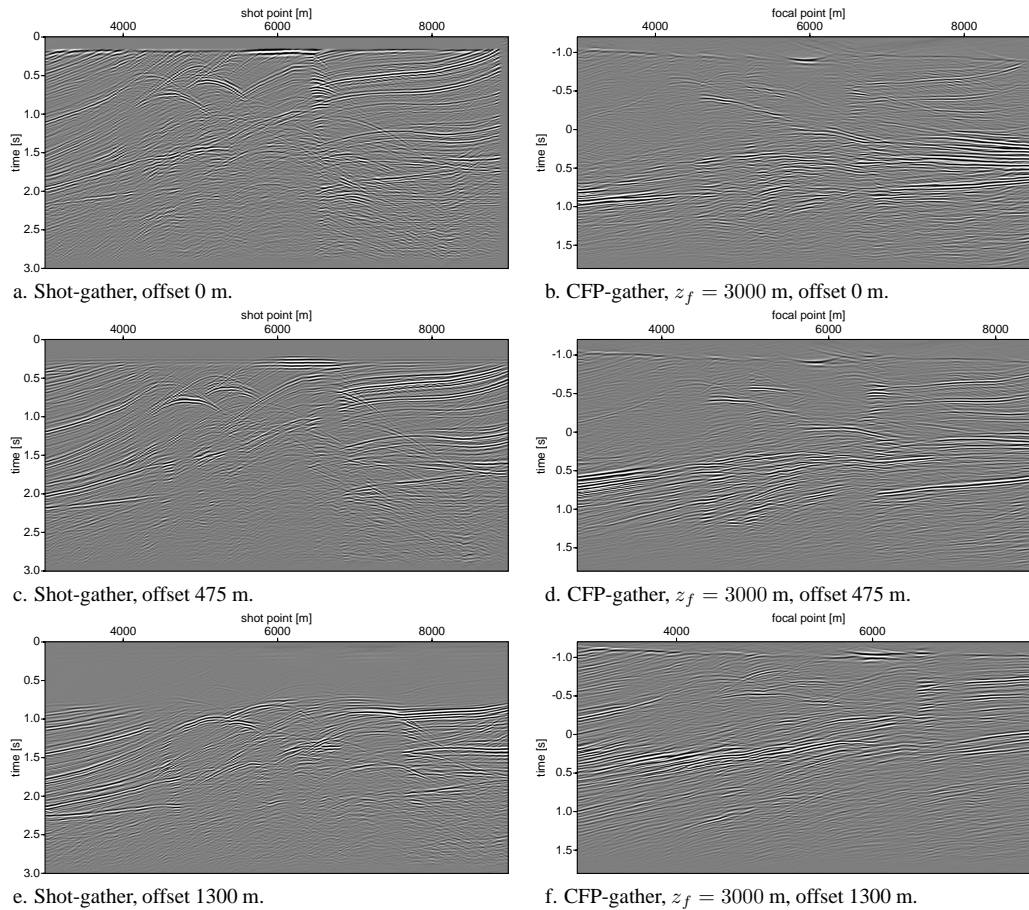


Fig. 13.6 Comparison between shot- and CFP-offset (focus depth $z_f = 3000$ m) gathers. The CFP-based offset gather gives a better image of the deeper subsurface than shot-based offset gathers. This favourable property will be used in the CFP-based image gathers.

13.4.1 Results on the 2D Marmousi model

In Figure 13.8 six conventional shot record migration results are shown. For the left hand-side pictures all available shots were used, and for the right hand-side 1/4 of the total shots was used only. For pictures c and d Gaussian noise has been added to the input shot records with a signal-to-noise ratio of 2, and for e and f with a ratio of 1. Figure 13.8a shows the full prestack migration result using all 240 shots of the Marmousi data set ($\Delta x_s = 25$ m), Figure 13.8b shows the image for $\Delta x_s = 100$ m. The difference in image quality between Figures 13.8a and b can hardly be observed, but the computation time for Figure 13.8b is four times smaller. For the results based on the noisy data, the effect of using less shot records is visible in terms of a lower signal to noise ratio in the migration result. Compared to Figure 13.8e, Figure 13.8f has a much lower image quality.

In Figure 13.9 the results for CFP-gather migration are shown. The focal points are chosen

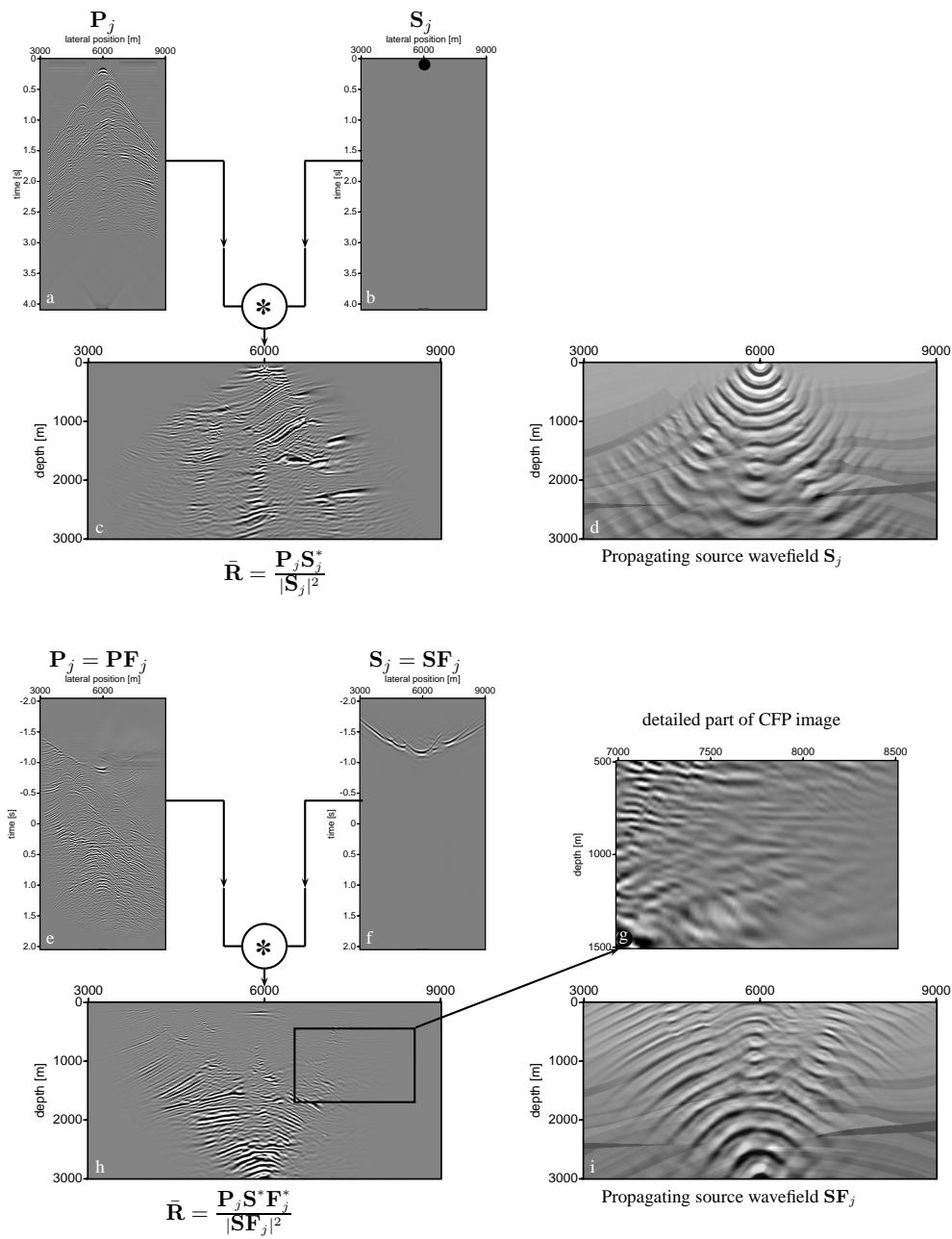


Fig. 13.7 Comparison between a migrated shot record (top) and a migrated CFP-gather (bottom). Picture a show a shot record and b its source wavefield. In CFP-gather migration the shot record (a) is replaced by the CFP-gather (e) and the source (b) is replaced by the focusing operator (f). In this example the focal point of the CFP-gather is chosen at $z_f = 3000$ m. Note the large difference in illumination between the image of shot record migration in c and CFP gather migration in h.

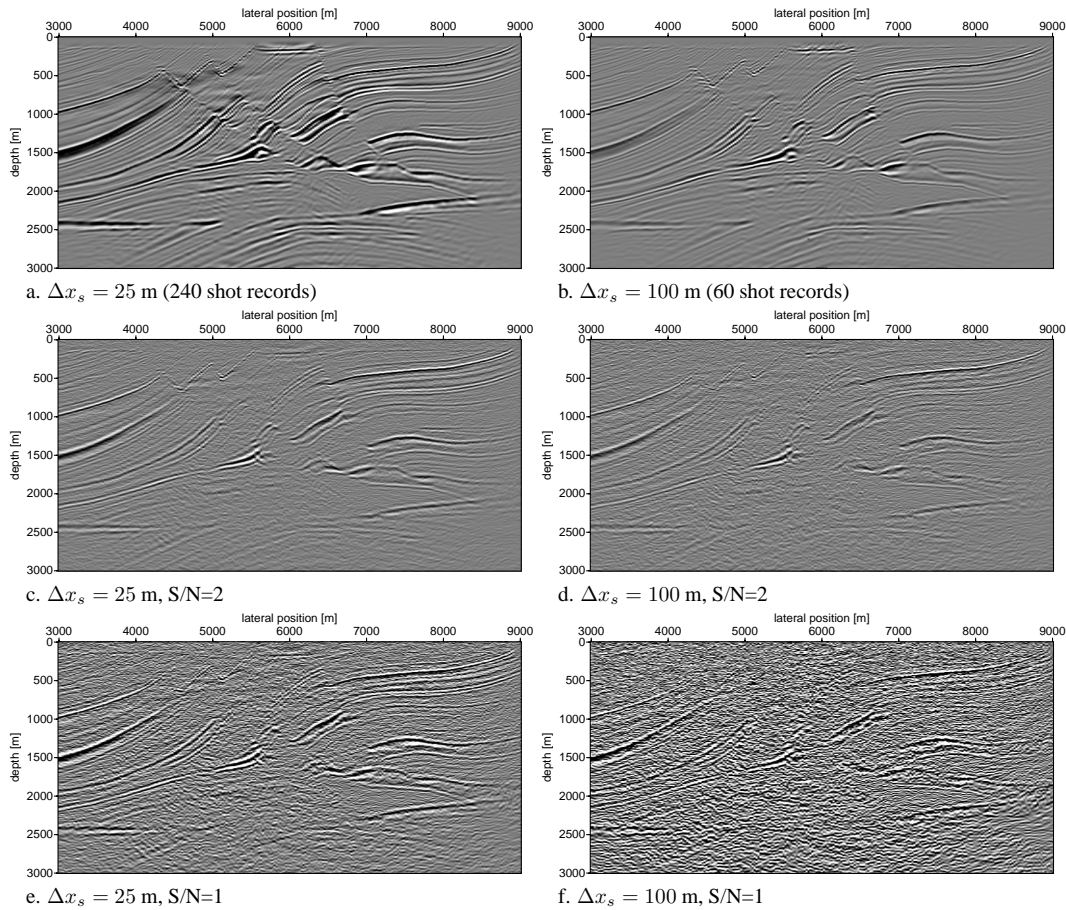


Fig. 13.8 Conventional shot record migration using a different shot sampling intervals (Δx_s), and different S/N ratio's. For the migration the correct velocity model has been used. The left figures are based on all 240 shots, the right pictures are based on 60 shots. Figures a,b are comparable in image quality, Figures e and f are clearly different. Due to the use of all shot records e has a better reduction of the noise than f.

at a depth of $z = 3000$ m, with different lateral distances between the focal points at that depth. For the left hand-side pictures 240 focal points are used ($\Delta x_f = 25$ m), for the right hand side pictures 60 focal points only ($\Delta x_f = 100$ m). The migrations in figures 13.8 and 13.9 are carried out with different noise levels added to the input shot records. Comparing the noise-added CFP-gather migration results of Figures 13.9 with the noise-added shot record migration results in Figure 13.8, the CFP-gather migration has a much better signal to noise ratio, because the noise has already been reduced by Fresnel-zone stacking. The closer we approach the focal depth boundary (here $z_f = 3000$ m) the more effective this property is.

Related to these observations one could design an operator in such a way that all the Fresnel zones, for a certain focal area in the true model (which exact position is not relevant), are present in the CFP-gather. The Fresnel zones which are present are then not summed up to

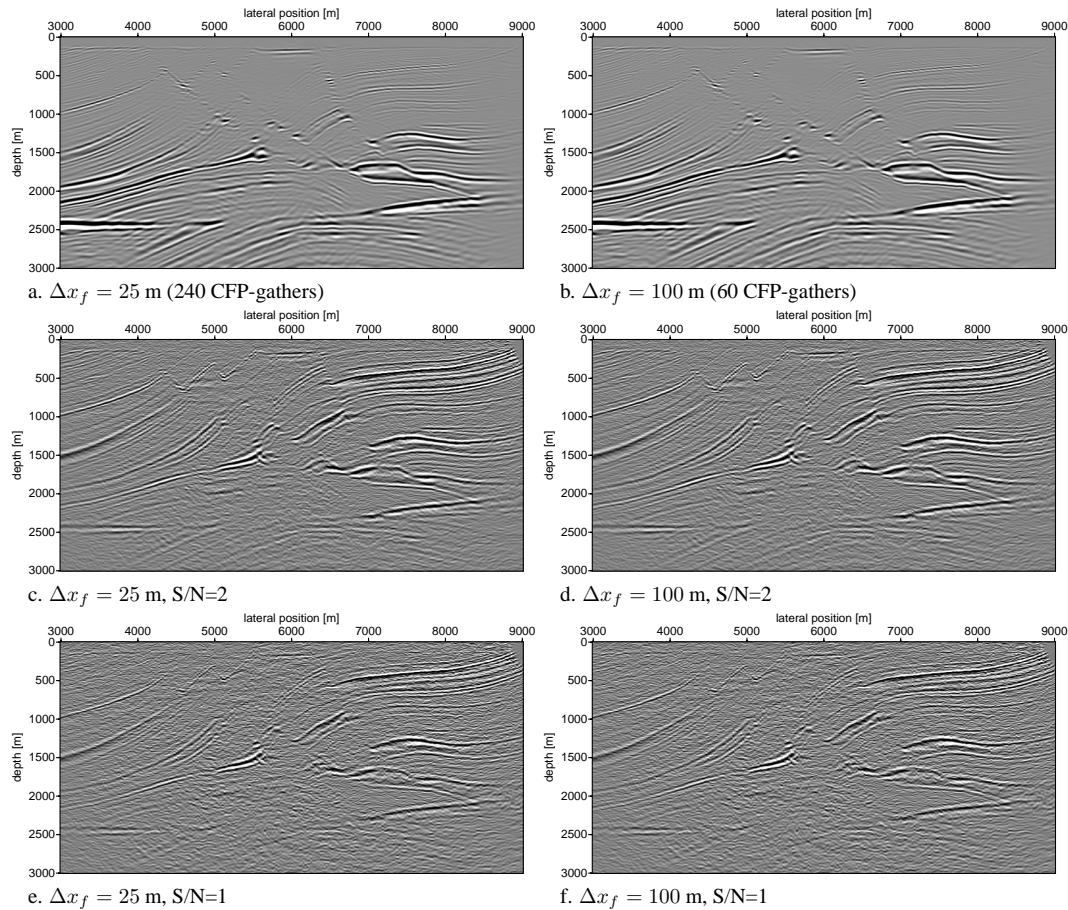


Fig. 13.9 CFP-gather migration using different focal point sampling intervals (Δx_f) at $z = 3000$ m, and different S/N ratio's. For the focusing operators the correct velocity model has been used. Figures e and f have comparable quality. This is in contrast with Figure 13.8. Using CFP, the noise reduction has already taken place in the focusing step by Fresnel-zone stacking, and migration of less CFP-gathers still gives a good S/N ratio.

an optimal stack, but at least they have a non-vanishing contribution in the CFP-gather and hence this energy can be migrated. An example of such an operator is an operator modelled in a very smooth velocity model. The smoothed velocity model has been made such that no multi-arrivals occurs in the one-way wavefields. The effect of using this operator in the construction of a CFP-gather is shown in Figure 13.10. The top part, representing shot record migration, shows that using this smoothed model breaks down the shot migration result; a lot of unmigrated events, observed as smiles, are still present. The CFP operator ($S_j = SF_j$, picture f) calculated in this smoothed model looks very simple compared to the one in Figure 13.7f. For the migration of the CFP-gather, the true model has to be used again to calculate the correct image. As stated before, as long as the CFP-gather and its focal source are consistent, they may be based on a velocity model that is different from the true model. Compared to

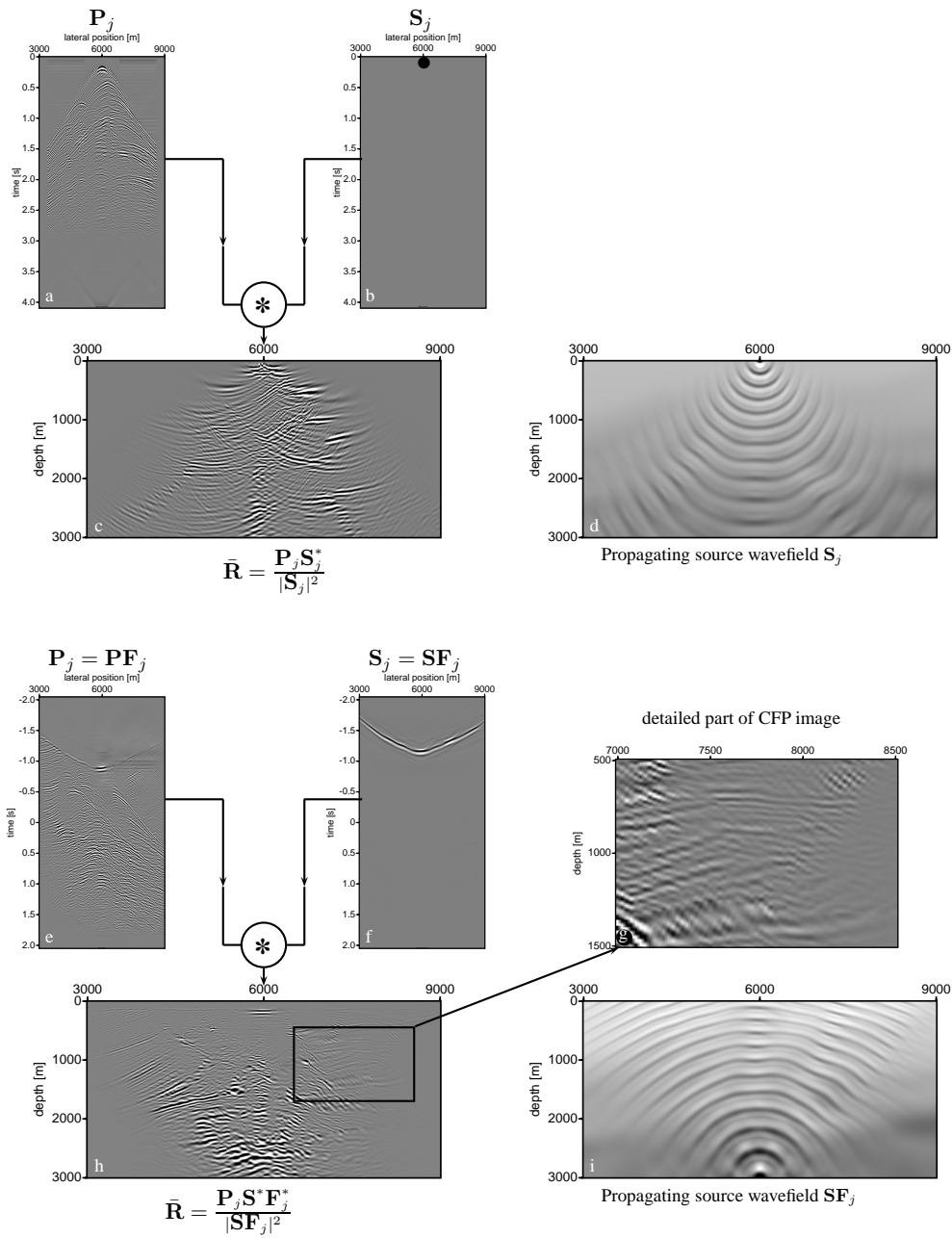


Fig. 13.10 Migration carried out with an averaged ($300 \times 300 \text{ m}^2$ smoothing operator) velocity model. The image of the shot record migration (c) contains a lot of unmigrated events, observed as smiles. In the migration of CFP-gathers a different velocity model is used for the focal operator (f) and in imaging (h). For the computation of the focal operator the smooth model was used. For the CFP-gather migration the true model was used. In the imaging step the focal operator is cancelled out.

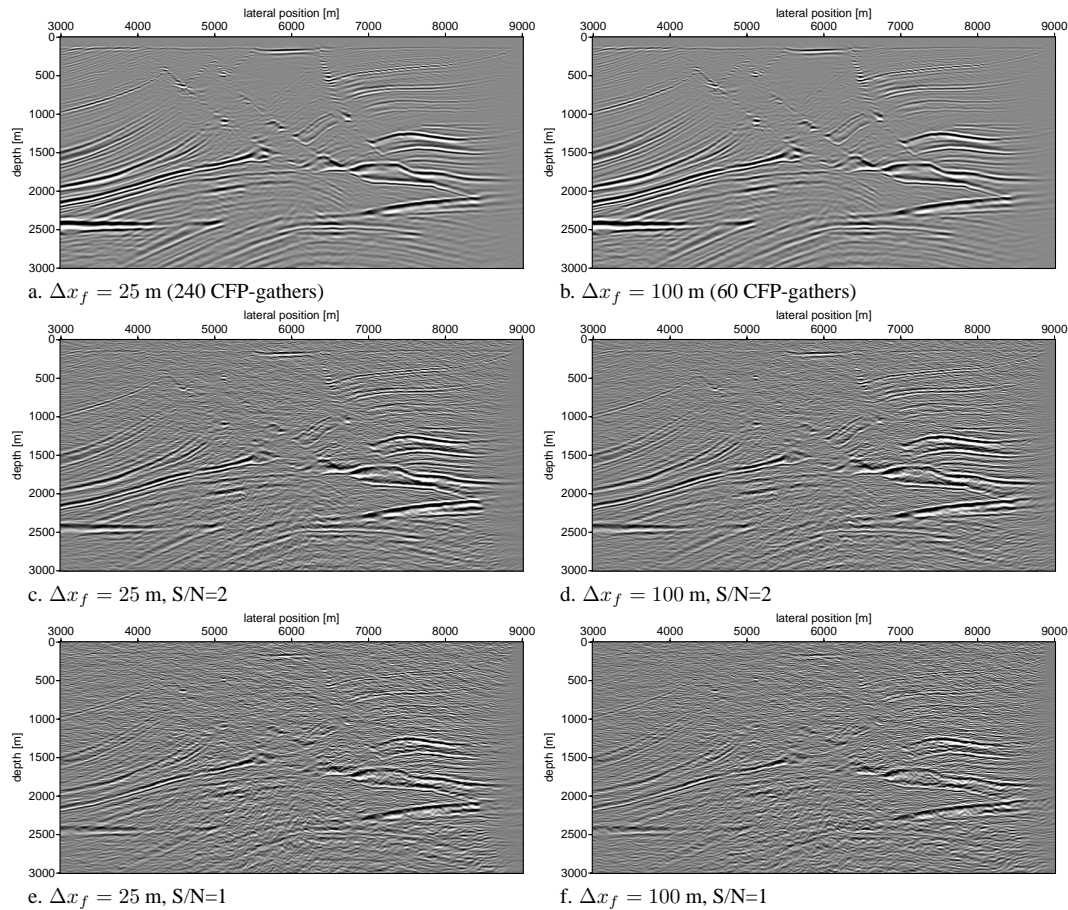


Fig. 13.11 Migration of CFP-gathers using different focal point sampling intervals (Δx_f) at $z = 3000$ m, and different S/N ratio's. The velocity model to generate the focal operators and the CFP-gathers has been smoothed (300×300 m² smoothing operator). For the actual migration the unsmoothed model is used.

Figure 13.7h the CFP migrated image in Figure 13.10h shows more imaged reflectors (for example look at the area around $x = 8000$ m, $z = 1000$ m and compare the zoomed in part (g) of the CFP image). Using this 'smooth' focusing operator, the CFP-gather contains Fresnel zones of more reflectors. In addition, the 'smooth' focusing operator has not one focal point but a focal area.

The result of CFP-gather migration with operators modeled in a smooth velocity model is shown in Figure 13.11. For these experiments the CFP-gathers are constructed with an operator modeled in a smoothed velocity model, but the CFP-gather migration is carried out with the correct model.

An important difference between shot-record and CFP-gather migration can be observed in image gathers, constructed from migrated shot records and migrated CFP-gathers. The image

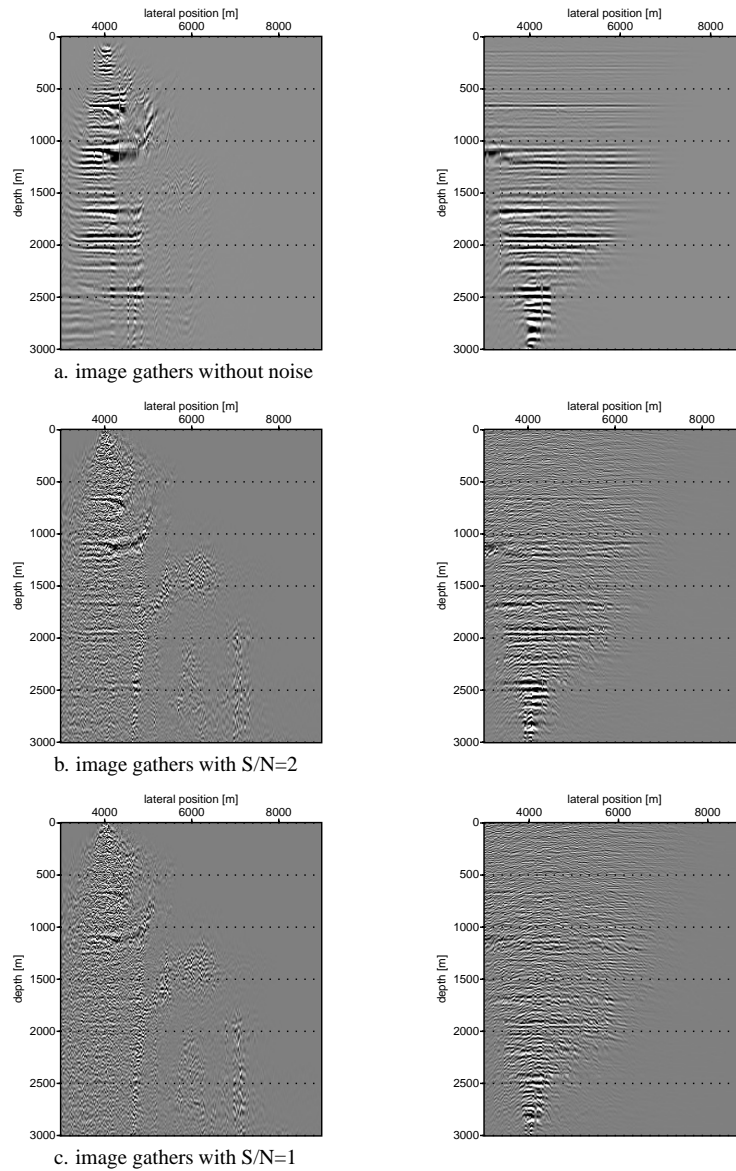


Fig. 13.12 Image gathers for shot record migration (left pictures) and CFP-gather migration (right pictures) at $x = 4000$ m for different noise levels. The focal depth for the CFP gathers is $z_f = 3000$ m. As expected, the CFP-based image gathers have better continuity of the events and the signal to noise ratio is higher. The correct model has been used to calculate the focal operators and to carry out the migration.

gathers for the CFP-gather migration are constructed in a similar way as the image gathers build up from shots: every migrated CFP-gather has a contribution to the image gather at a chosen lateral position.

The image gathers of Figures 13.12 and 13.13 show that the CFP-image gathers (right hand-side) have a better lateral continuity compared to the shot record image gathers (left hand-

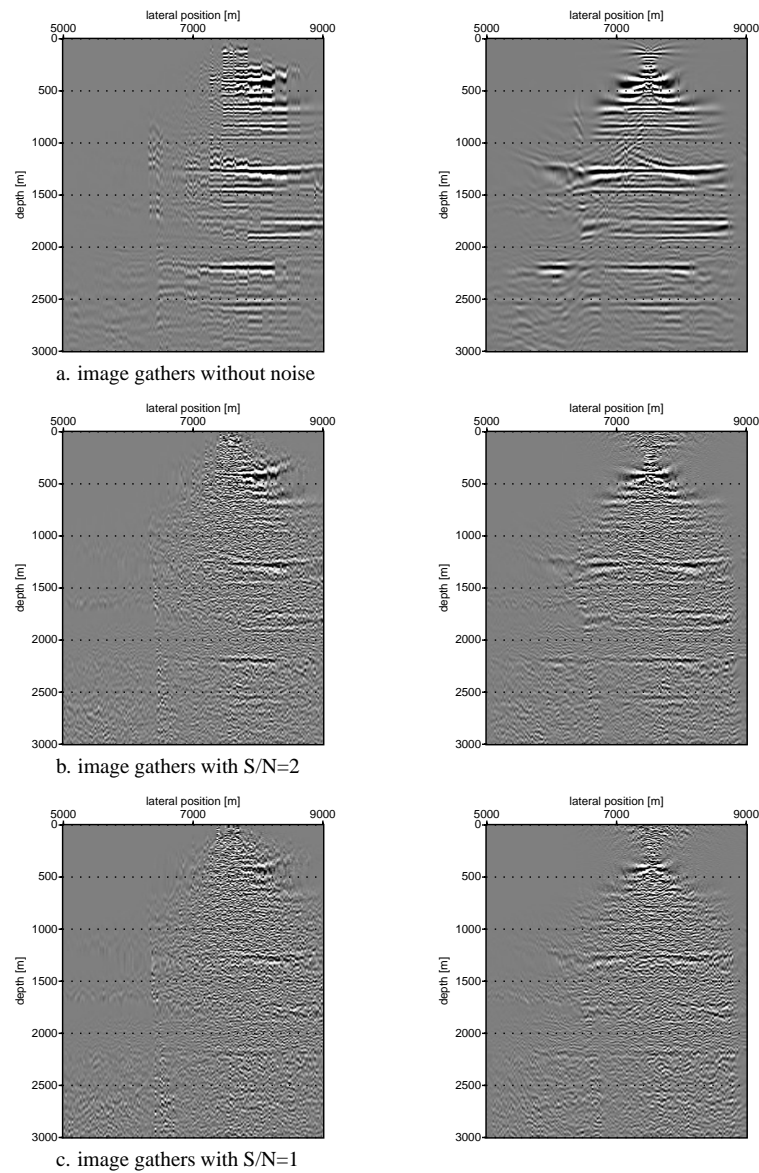


Fig. 13.13 Image gathers for shot record migration (left pictures) and CFP-gather migration (right pictures) at $x = 7500$ m for different noise levels. The focal depth for the CFP gathers is $z_f = 300$ m. The CFP-based image gathers have better continuity of the events and the signal to noise ratio is higher. The correct model has been used to calculate the focal operators and to carry out the migration.

side). Close to the focal point of the CFP-gathers, at $z = 3000$ m in Figure 13.12 and $z = 300$ m in Figure 13.13, the lateral continuity shrinks due to the focusing of the source energy. The S/N ratio in the image gather from CFP-gathers (pictures b and c) is higher and therefore better suited for velocity analysis. The summation over the Fresnel zone reduces the spatially incoherent noise. To reduce the coherent noise extra Fresnel zone filters could be applied.

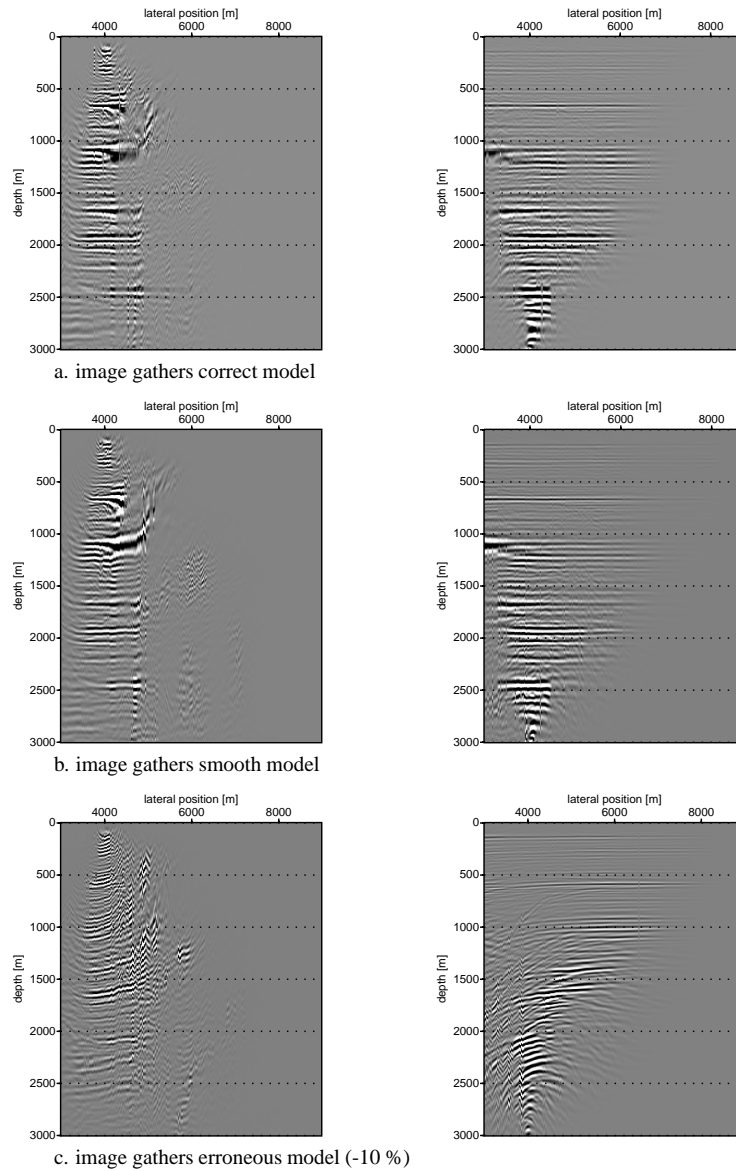


Fig. 13.14 Image gathers for shot record migration (left pictures) and CFP-gather migration (right pictures) at $x = 4000$ m. The focal depth for the CFP gathers is $z_f = 3000$ m. A smoothed version of the velocity model has been used in b, and an erroneous macro velocity model (-10 % for all velocities) in c. The smooth and erroneous model have been used to calculate the focal operators and to carry out the migration.

Note that in the CFP-based image gathers source-receiver reciprocity has been taken into account.

The reflectors which are far away from the focal point in the CFP image gather will have a S/N ratio comparable to that of shot record migration. This is caused by the fact that only at the focal point the Fresnel zone stack is optimal (will have its largest lateral extent). For all other

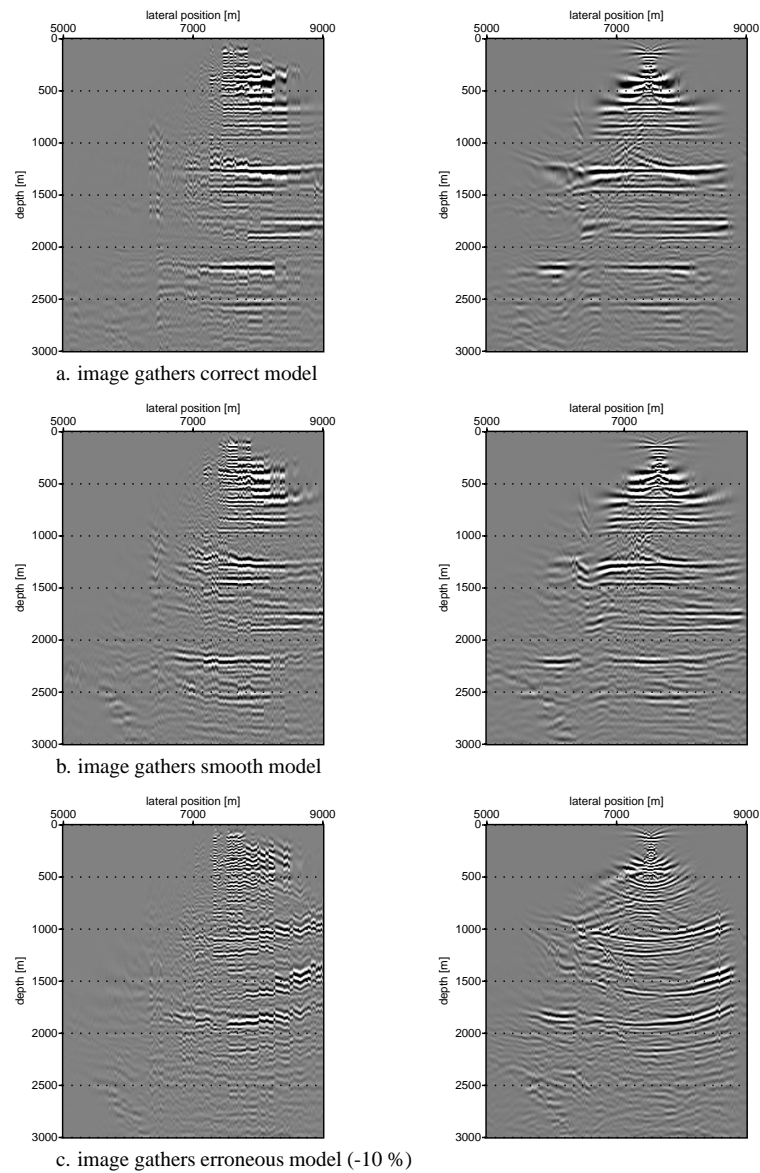


Fig. 13.15 Image gathers for shot record migration (left pictures) and CFP-gather migration (right pictures) at $x = 7500$ m. The focal depth for the CFP gathers is $z_f = 300$ m. A smoothed version of the velocity model has been used in b, and an erroneous macro velocity model (-10 % for all velocities) in c. The smooth and erroneous model have been used to calculate the focal operators and to carry out the migration.

points this zone will be smaller, and consequently a smaller improvement of the S/N ratio.

CFP image gathers can also be used for velocity analysis. Figures 13.14 and 13.15 show image gathers where an erroneous velocity model has been used. The CFP-gather shows the velocity errors more pronounced, and errors can be followed at a larger lateral distance. The shot-based image gathers in Figure 13.15 show for the deeper events discontinuities caused

by the shallower parts in the model. In the CFP-based image gathers these discontinuities are absent, because the shallow subsurface was already accounted for by the focusing operator. By choosing different focal depths for the CFP image gathers, at $z = 3000$ m in Figure 13.14 and $z = 300$ m in Figure 13.15, different parts of the model can be analysed in more detail.

13.5 Conclusions

CFP gathers are constructed from all available shot records and are related to a focus in the subsurface. CFP-gathers can be considered as shot records generated by a focal source array and can be migrated with a shot record migration algorithm.

Focusing involves Fresnel zone stacking. Therefore, CFP-gathers have a higher signal-to-noise ratio than shot records. Since focusing removes spatial phase from the data, CFP gathers contains simpler events than the original shot record.

In a CFP image gather, being based on migrated CFP-gathers, each migrated trace contains multi-fold data. The result is easier to interpret than image gathers based on single-fold migrated field records. Focal operators can be generated in a reference medium that may be different from the medium used in the migration process.

13.6 Future plans

We are now investigating the combination of CFP-gathers at different depth levels.

13.7 References

- Berkhout, A. J., and Verschuur, D. J., 2000, Internal multiple removal - boundary-related and layer-related approach: 62th Ann. Internat. Mtg., European Association of Geoscientist & Engineers, Annual Meeting Abstracts, L-56.
- Berkhout, A. J., 1980, Imaging of acoustic energy by wave field extrapolation: Elsevier, Amsterdam.
- Berkhout, A. J., 1982, Imaging of acoustic energy by wave field extrapolation (2nd edition): Elsevier, Amsterdam.
- Berkhout, A. J., 1992, Areal shot record technology: *Journal of Seismic Exploration*, **1**, no. 2, 251-264.
- Berkhout, A. J., 1997, Pushing the limits of seismic imaging, part I: Prestack migration in terms of double dynamic focusing: *Geophysics*, **62**, 937-953.
- Blacquière, G., 1989, 3D wave field extrapolation in seismic depth migration: Ph.D. thesis, Delft University of Technology.

- Bolte, J., Verschuur, D., and Hegge, R., 1999, Cfp operator estimation and inversion demonstrated on a field data set, part i: Operator updating: 69th Ann. Internat. Mtg., Society Of Exploration Geophysicists, Annual Meeting Abstracts, 1711–1714.
- Brisbourne, A., Pointer, T., and Crook, H., 2000, Improved imaging beneath complex near-surface structure using cfp velocity analysis: 62th Ann. Internat. Mtg., European Association of Geoscientist & Engineers, Annual Meeting Abstracts, L–34.
- Hegge, R., Duijndam, A., Bolte, J., and Fokkema, J., 1999, Cfp operator estimation and inversion demonstrated on a field data set, part ii: Velocity estimation: 69th Ann. Internat. Mtg., Society Of Exploration Geophysicists, Annual Meeting Abstracts, 1500–1503.
- Holberg, O., 1988, Towards optimum one-way wave propagation: *Geophysical Prospecting*, **36**, 99–114.
- Kabir, M. M. N., and Verschuur, D. J., 1997, Velocity analysis of the complex subsurface using the common focus point technology: 67th Ann. Internat. Mtg., Society Of Exploration Geophysicists, Annual Meeting Abstracts, 1822–1825.
- Kelamis, P., Verschuur, D., Berkhout, A., and Erickson, K., 1999, Velocity-independent datuming of seismic data: 69th Ann. Internat. Mtg., Society Of Exploration Geophysicists, Annual Meeting Abstracts, 441–444.
- Rietveld, W. E. A., 1995, Controlled illumination in prestack seismic migration: Ph.D. thesis, Delft University of Technology.
- Thorbecke, J., Wapenaar, K., and Swinnen, G., 2004, Design of one-way wavefield extrapolation operators, using smooth functions in wlsq optimization: *Geophysics*, **69**, 1037–1045.
- Thorbecke, J. W., 1997, Common focus point technology: Ph.D. thesis, Delft University of Technology.
- Versteeg, R., and Grau, G., 1991, The Marmousi experience : 53th Ann. Internat. Mtg., Eur. Assoc. Expl. Geophys., EAEG workshop on practical aspects of seismic data inversion.